

# SGBEM-FEM Alternating Method for Analyzing 3D Non-planar Cracks and Their Growth in Structural Components<sup>1</sup>

G.P.Nikishkov<sup>2</sup>, J.H.Park<sup>3</sup> and S.N.Atluri<sup>2</sup>

**Abstract:** An efficient and highly accurate, Symmetric Galerkin Boundary Element Method - Finite Element Method - based alternating method, for the analysis of three-dimensional non-planar cracks, and their growth, in structural components of complicated geometries, is proposed. The crack is modeled by the symmetric Galerkin boundary element method, as a distribution of displacement discontinuities, as if in an infinite medium. The finite element method is used to perform the stress analysis for the uncracked body only. The solution for the structural component, containing the crack, is obtained in an iteration procedure, which alternates between FEM solution for the uncracked body, and the SGBEM solution for the crack in an infinite body. Numerical procedures, and the attendant Java code, are developed for the evaluation of stress intensity factors, and fatigue crack growth modeling. Examples for non-planar cracks in infinite media, and for planar cracks in finite bodies, as well as their growth under fatigue, demonstrate the accuracy of the method.

**keyword:** SGBEM, FEM, alternating, 3D non-planar crack.

## 1 Introduction

The calculation of fracture mechanics parameters (such as the stress intensity factors of Mode I, II and III), for arbitrary three-dimensional surface and internal cracks, remains an important task in the structural integrity assessment and damage tolerance analysis [Atluri (1997)].

The finite element method (FEM) and the boundary element method (BEM) were used in earlier years, successfully for this purpose.

The finite element procedures for fracture mechanics analysis are well established. The use of energetic methods and in particular the equivalent domain integral method [Nikishkov and Atluri (1987); Shivakumar and Raju (1992)] allows one to obtain fracture mechanics parameters with acceptable accuracy. Unfortunately, a serious difficulty in applying the finite element method to the analysis of three-dimensional cracks, lies in the mesh generation. The human labor cost is extremely high for creating appropriate meshes for arbitrary non-planar cracks in structural components of arbitrary geometry.

In the boundary element method for linear problems, the mesh should be generated only for the boundary of the structure, and for the crack surface. Consequently, it is simpler to create a boundary element mesh, in comparison to a finite element mesh for a body with a crack. However, for a surface crack, it is necessary to maintain mesh compatibility between the mesh on the crack surface, and that on the boundary of the structure. If it is necessary to analyze cracks of different sizes, both the crack-surface mesh and the mesh for the surface of the structure, should be modified. The traditional (collocation) boundary element method has certain features, which makes it suitable for the solution of crack problems. Recent publications on the dual boundary element method [Cisilino and Aliabadi (1999)] can serve as an example of application of traditional BEM to linear and non-linear fracture mechanics problems. Despite its well understood advantages for some problems, the traditional BEM has still some features that makes it less attractive for use in fatigue-growth analysis of non-planar cracks. Among them it is possible to mention the non-symmetrical matrix of the equation system, and the hypersingular kernels contained in the traditional integral relations.

<sup>1</sup> This paper is presented in honor of the 90th birthday of the distinguished UCLA Academician, Professor T.H. Lin, whose contributions to the mechanics of fatigue are seminal and monumental.

<sup>2</sup> Center for Aerospace Research & Education  
7704 Boelter Hall, UCLA  
Los Angeles, CA 90095-1600, USA

<sup>3</sup> Dept. of Safety Engineering  
Chungbuk National University  
Chungbuk 361-763, Korea

An approach combining the traditional hypersingular boundary element method, and the finite element method, is used by Keat, Annigeri and Cleary (1988) for the solution of two- and three-dimensional fracture mechanics problems. Based on the superposition principle, the authors employ a direct method for creating a system of equations for the fracture mechanics problem. An obvious disadvantage of this approach is the large size of the matrices that characterize the interaction between the finite element and the boundary element global matrices, and consequently the large solution times on a digital computer.

The symmetric Galerkin boundary element method (SGBEM) [Bonnet, Maier and Polizzotto (1998)], is a way of satisfying the boundary integral equations of elasticity in a Galerkin weak form, as opposed to the method of collocations that is generally used to satisfy the integral equations in the traditional BEM. The SGBEM helps to overcome some drawbacks of the traditional boundary element approach. The SGBEM is characterized by weakly singular kernels. After a special transformation, which removes the singularity from kernels, the boundary element matrices can be integrated with the use of usual Gaussian quadrature rule.

In this paper, the SGBEM-FEM alternating method, for the analysis of non-planar cracks in finite bodies, is presented. The method alternates between the FEM solution for an uncracked structural component of a finite geometry, and the SGBEM solution for a crack in an infinite body. The crack is modeled as a distribution of displacement discontinuities. The crack surface is discretized by quadratic eight-noded boundary elements. Quarter-point singular elements are placed near the crack front. With the use of the proposed procedure the stress intensity factors for planar and non-planar cracks in infinite media, and for embedded and surface cracks in finite bodies, are calculated. A comparison of the results with the published solutions shows that the SGBEM-FEM alternating method is very efficient and highly accurate for analyzing non-planar cracks. A numerical procedure for analyzing the fatigue crack growth of nonplanar cracks is also developed. The direction and magnitude of crack advance are based on the direction and magnitude of the  $J$ -integral vector. Results for nonplanar fatigue crack growth of an inclined elliptical precrack are provided.

The present paper for treating non-planar cracks of arbitrary geometry, in finite-sized structural components of

arbitrary geometry, represents a further refinement of the Shwartz-Neumann alternating technique developed over the years [Atluri (1997); Nishioka and Atluri (1983), and Vijaykumar and Atluri (1981)]. In these earlier papers, only cracks of (part)-elliptical geometries were considered; and the alternating was between the analytical solution for an elliptical crack in an infinite body [Vijaykumar and Atluri (1981)] and the finite element solution for an uncracked finite body. In that sense, the Vijaykumar and Atluri (1981) solution of the earlier alternating method, is now replaced by the SGBEM solution for a non-planar crack of arbitrary geometry, in the present paper. The next logical step in this series of developments is to replace the finite element solution for the uncracked finite body, with a meshless local Petrov-Galerkin (MLPG) solution for the uncracked finite body [Atluri and Zhu (1998); Kim and Atluri (2000), and Lin and Atluri (2000)]. This will be forthcoming.

## 2 Symmetric Galerkin Boundary Element Method

### 2.1 Governing integral equations

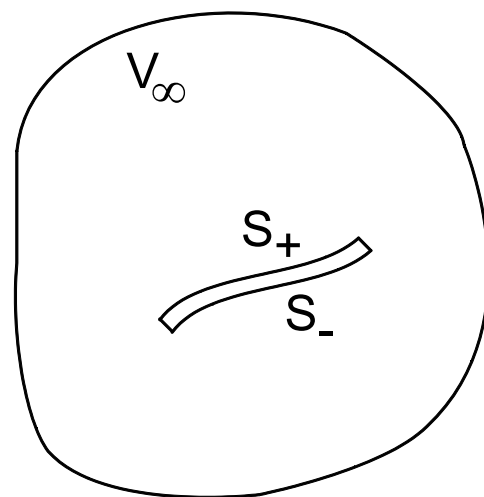


**Figure 1** : Crack as displacement discontinuity in an infinite body.

Consider an infinite three-dimensional body containing a non-planar crack of arbitrary geometry as shown in Fig. 1. A distributed load is applied at the crack surface. The crack can be described by a distribution of *displacement discontinuity*, with components  $u_i = u_i^{S_+} - u_i^{S_-}$  ( $i = 1 \dots 3$ ), where  $S_+$  and  $S_-$  are two crack surfaces.

The following weakly-singular boundary integral equation is valid for the crack [Bonnet, Maier and Polizzotto (1998); Xu and Ortiz (1993); Li and Mear (1998), Li, Mear and Xiao (1998)]:

$$\begin{aligned}
 & - \iint_{S S} D_{\alpha} u_i^*(\mathbf{z}) C_{\alpha i \beta j}(\xi - \mathbf{z}) D_{\beta} u_j(\xi) dS(\xi) dS(\mathbf{z}) \\
 & = \int_S u_i^*(\mathbf{z}) t_i dS(\mathbf{z})
 \end{aligned}$$

Here  $S = S_+$  is one of crack surfaces;  $u_i$  are displacement discontinuities for the crack surface;  $u_i^*$  are the components of a continuous test function; and  $t_i$  are crack face tractions.

The two-point weakly singular kernel is given by the following expression:

$$\begin{aligned}
 C_{\alpha i \beta j}(\zeta) &= \frac{\mu}{4\pi(1-\nu)r} \left( (1-\nu)\delta_{i\alpha}\delta_{j\beta} + 2\nu\delta_{i\beta}\delta_{j\alpha} - \delta_{ij}\delta_{\alpha\beta} - \frac{\zeta_i\zeta_j}{r^2}\delta_{\alpha\beta} \right) \\
 \zeta &= \xi - \mathbf{z} \\
 r^2(\zeta) &= \zeta_i\zeta_i
 \end{aligned}$$

where  $\nu$  is Poisson's ratio and  $\mu$  is the shear modulus.

A tangential operator  $D_{\alpha}$  is defined as follows:

$$\begin{aligned}
 D_{\alpha} &= \frac{1}{J} \left( \frac{\partial}{\partial \eta_1} \frac{\partial x_{\alpha}}{\partial \eta_2} - \frac{\partial}{\partial \eta_2} \frac{\partial x_{\alpha}}{\partial \eta_1} \right) \\
 J &= |\mathbf{s} \times \mathbf{t}| \\
 \mathbf{s} &= \partial \mathbf{x} / \partial \eta_1, \quad \mathbf{t} = \partial \mathbf{x} / \partial \eta_2
 \end{aligned}$$

where  $\eta_1, \eta_2$  are the surface coordinates on the crack surface, and  $\mathbf{s}, \mathbf{t}$  are vectors in the plane that is tangent to the crack surface.

### 2.2 Displacement and stress fields

The displacement field around the crack can be determined, with the use of Somigliana's identity:

$$u_p(\mathbf{x}) = - \int_S n_i(\xi) S_{ij}^p(\xi - \mathbf{x}) u_j(\xi) dS(\xi) \quad (4)$$

Stresses are determined by the expression:

$$\sigma_{kl}(\mathbf{x}) = - \int_S E_{klpq} e_{iqm} S_{ij}^p(\xi - \mathbf{x}) D_m u_j(\xi) dS(\xi) \quad (5)$$

Here  $E_{klpq}$  is the elasticity tensor;  $e_{iqm}$  is the permutation symbol and  $S_{ij}^p$  is the stress fundamental solution:

$$\begin{aligned}
 & S_{ij}^p(\zeta) \\
 &= \frac{1}{8\pi(1-\nu)r^2} \left( \frac{(1-2\nu)}{r} (\zeta_p\delta_{ij} - \zeta_i\delta_{pj} - \zeta_j\delta_{pi}) - \frac{3\zeta_p\zeta_i\zeta_j}{r^3} \right)
 \end{aligned} \quad (6)$$

### 2.3 Discretization of the integral equation

We assume that the crack is partitioned into boundary elements. Displacement discontinuities and tractions are defined at element nodes, and are interpolated inside the elements with the use of shape functions  $N_a$ :

$$\begin{aligned}
 u_i &= N_a(\eta_1, \eta_2) u_{ia} \\
 t_i &= N_a(\eta_1, \eta_2) t_{ia}
 \end{aligned} \quad (7)$$

where  $i = 1, 2, 3$  is the global coordinate subscript;  $a$  is the node number;  $\eta_1, \eta_2$  are element local coordinates. With the use of a parametric representation of displacement discontinuities and tractions, we can rewrite the integral equation (1) in the following discretized form:

$$- \iint_{S S} C_{\alpha i \beta j} D_{\alpha} N_a(z) D_{\beta} N_b(\xi) dS(\xi) dS(z) u_{jb} = \int_S N_a N_q dS(z) t_{iq} \quad (8)$$

or in the following matrix-vector form:

$$K_{iajb} u_{jb} = H_{aq} t_{iq} \quad (9)$$

The global equation system is composed of the element matrices:

$$k_{iajb}^{mn} = - \iint_{S_m S_n} C_{\alpha i \beta j} D_{\alpha} N_a(z) D_{\beta} N_b(\xi) dS(\xi) dS(z) \quad (10)$$

$$h_{aq}^m = \int_{S_m} N_a N_q dS(z) \quad (11)$$

The  $m$ th hyper-line (corresponding to degrees of freedom of one boundary element) of the global equation system is written as:

$$\sum_n k_{iajb}^{mn} u_{jb} = h_{aq}^m t_{iq} \quad (12)$$

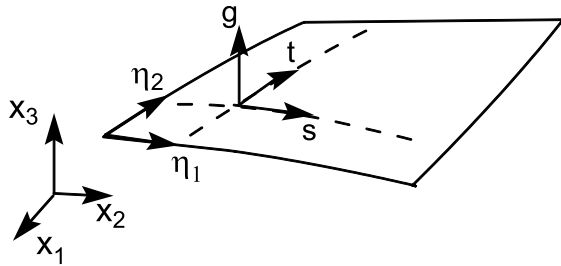


**Figure 2** : Boundary element with a local coordinate system.

The tangential operator  $D_\alpha$  is applied twice to element shape functions in Eq. (10). Consider the computation of the expression  $D_\alpha N_a$  for a boundary element, as shown in Fig. 2. Vectors  $\mathbf{s}$  and  $\mathbf{t}$  which are tangent to the lines of constant value of the local coordinates  $\eta_1, \eta_2$  are equal to:

$$\mathbf{s} = \left\{ \frac{\partial x_1}{\partial \eta_1} \quad \frac{\partial x_2}{\partial \eta_1} \quad \frac{\partial x_3}{\partial \eta_1} \right\}, \quad \mathbf{t} = \left\{ \frac{\partial x_1}{\partial \eta_2} \quad \frac{\partial x_2}{\partial \eta_2} \quad \frac{\partial x_3}{\partial \eta_2} \right\} \quad (13)$$

Assuming that the coordinate interpolation is performed with the same shape functions as used for displacement interpolation, the partial derivatives of the global coordinates in respect to local coordinates can be easily calculated in the following way:

$$\frac{\partial x_i}{\partial \eta_j} = \frac{\partial N_a}{\partial \eta_j} x_{ia} \quad (14)$$

where  $a$  is the node number. The Jacobian  $J$  is equal to the length of a vector  $\mathbf{g}$ , which is a vector product of vectors  $\mathbf{s}$  and  $\mathbf{t}$ :

$$g_1 = \frac{\partial x_2}{\partial \eta_1} \frac{\partial x_3}{\partial \eta_2} - \frac{\partial x_3}{\partial \eta_1} \frac{\partial x_2}{\partial \eta_2} \quad (15)$$

$$g_2 = \frac{\partial x_3}{\partial \eta_1} \frac{\partial x_1}{\partial \eta_2} - \frac{\partial x_1}{\partial \eta_1} \frac{\partial x_3}{\partial \eta_2}$$

$$g_3 = \frac{\partial x_1}{\partial \eta_1} \frac{\partial x_2}{\partial \eta_2} - \frac{\partial x_2}{\partial \eta_1} \frac{\partial x_1}{\partial \eta_2}$$

$$J(\eta_1, \eta_2) = |\mathbf{g}| = \sqrt{g_1^2 + g_2^2 + g_3^2} \quad (16)$$

The derivatives of the shape functions with respect to the local coordinates are found explicitly, since the shape functions are expressed in terms of local coordinates.

#### 2.4 Integration of element matrices

A typical integral of a matrix entry, for the combination of boundary elements  $n$  and  $m$ , can be written in the following form:

$$I_{nm} = \int_{S_n} \int_{S_m} f(\mathbf{x}, \tilde{\mathbf{x}}) dS_x dS_{\tilde{x}} = \int_0^1 \int_0^1 \int_0^1 \int_0^1 F(\mathbf{x}(\eta_1, \eta_2), \tilde{\mathbf{x}}(\tilde{\eta}_1, \tilde{\eta}_2)) d\eta_1 d\eta_2 d\tilde{\eta}_1 d\tilde{\eta}_2 \quad (17)$$

Taking into account that area elements can be presented in the form:

$$\begin{aligned} dS(\mathbf{x}) &= J(\mathbf{x}) d\eta_1 d\eta_2 \\ dS(\tilde{\mathbf{x}}) &= J(\tilde{\mathbf{x}}) d\tilde{\eta}_1 d\tilde{\eta}_2 \end{aligned} \quad (18)$$

and that the determinant of Jacobi matrix is contained in the expression for the tangential operator  $D_\alpha$  the integrand can be written as follows:

$$F = -C_{\alpha i \beta j} (N_{a,1} x_{\alpha,2} - N_{a,2} x_{\alpha,1}) (N_{b,1} \tilde{x}_{\beta,2} - N_{b,2} \tilde{x}_{\beta,1}) \quad (19)$$

$$N_{a,i} = \frac{\partial N_a}{\partial \eta_i}, \quad N_{b,i} = \frac{\partial N_b}{\partial \tilde{\eta}_i} \quad (20)$$

$$x_{a,i} = \frac{\partial x_a}{\partial \eta_i}, \quad \tilde{x}_{b,i} = \frac{\partial \tilde{x}_b}{\partial \tilde{\eta}_i} \quad (21)$$

The integral  $I_{nm}$  can be estimated using the Gaussian integration rule:

$$I_{nm} = \sum_i \sum_j \sum_k \sum_l F(\eta_{1i}, \eta_{2j}, \tilde{\eta}_{1k}, \tilde{\eta}_{2l}) w_i w_j w_k w_l \quad (22)$$

where  $\eta_{1i}, \eta_{2j}$  are abscissas of the Gaussian integration rule and  $w_i w_j$  are correspondent weights. While such an integration procedure is appropriate for a specific pair of elements, which have no common points, it can not provide sufficient accuracy for other elements, which are coincident or have one edge or one vertex in common.

An efficient approach to double area integration of weakly singular kernels is presented in References [Andra (1998); Erichsen and Sauter (1998)] for triangular boundary elements. The approach is based on coordinate transformations, which produce such a transformation Jacobian that it cancels the weak singularity of the kernel. We developed the corresponding integration approach for special cases of pairs of quadrilateral elements shown in Fig. 3; then we discovered that a convenient form of this integration was published independently by Frangi, Novati, Springhetti and Rovizzi (2000). For coincident elements and for elements with common edge or common vertex, the four-dimensional integration domain  $0 \leq \eta_1, \eta_2, \tilde{\eta}_1, \tilde{\eta}_2 \leq 1$  is divided into several integration subdomains. In each subdomain, a special coordinate transformation is introduced, which cancels the singularity. The integral  $I_{nm}$  for a special case is computed as a sum of subdomain integrals:

$$I_{nm} = \int_0^1 \int_0^1 \int_0^1 \int_0^1 \sum_{i=1}^s F(\mathbf{x}(\eta_1^i, \eta_2^i), \tilde{\mathbf{x}}(\tilde{\eta}_1^i, \tilde{\eta}_2^i)) J_i d\omega d\xi_1 d\xi_2 d\xi_3 \quad (23)$$

where  $s$  is the number of integration subdomains,  $\eta_1^i, \eta_2^i, \tilde{\eta}_1^i, \tilde{\eta}_2^i$  are local coordinates in subdomain  $i$ , which are expressed through integration variables  $0 \leq \omega, \xi_1, \xi_2, \xi_3 \leq 1$  and  $J_i$  is the subdomain transformation Jacobian. For the three special integration cases, the variables in Eq. (23) can be expressed as follows.

*Coincident elements*

Number of subdomains  $s = 8$ .

$i$	$\tilde{\eta}_1^i$	$\tilde{\eta}_2^i$	$\eta_1^i$	$\eta_2^i$
1	$v_3$	$v_4$	$v_{1+v_3}$	$v_{2+v_4}$
2	$v_3$	$v_{2+v_4}$	$v_{1+v_3}$	$v_4$
3	$v_{1+v_3}$	$v_{2+v_4}$	$v_3$	$v_4$
4	$v_{1+v_3}$	$v_4$	$v_3$	$v_{2+v_4}$
5	$v_4$	$v_3$	$v_{2+v_4}$	$v_{1+v_3}$
6	$v_{2+v_4}$	$v_3$	$v_4$	$v_{1+v_3}$
7	$v_{2+v_4}$	$v_{1+v_3}$	$v_4$	$v_3$
8	$v_4$	$v_{1+v_3}$	$v_{2+v_4}$	$v_3$

$$\begin{aligned} v_1 &= \omega \\ v_2 &= \xi_1 \omega \\ v_3 &= \xi_2 (1 - \omega) \\ v_4 &= \xi_3 (1 - \xi_1 \omega) \end{aligned}$$

$$J_i = \omega(1 - \omega)(1 - \xi_1 \omega)$$

*Elements with a common edge*

Number of subdomains  $s = 6$ .

$i$	$\tilde{\eta}_1^i$	$\tilde{\eta}_2^i$	$\eta_1^i$	$\eta_2^i$
1	$v_4$	$v_2$	$v_{1+v_4}$	$v_3$
2	$v_5$	$v_1$	$v_{5+v_2}$	$v_3$
3	$v_5$	$v_3$	$v_{5+v_2}$	$v_1$
4	$v_{1+v_4}$	$v_2$	$v_4$	$v_3$
5	$v_{5+v_2}$	$v_1$	$v_5$	$v_3$
6	$v_{5+v_2}$	$v_3$	$v_5$	$v_1$

$$\begin{aligned} v_1 &= \omega \\ v_2 &= \xi_1 \omega \\ v_3 &= \xi_2 \omega \\ v_4 &= \xi_3 (1 - \omega) \\ v_5 &= \xi_3 (1 - \xi_1 \omega) \end{aligned}$$

$$\begin{aligned} J_1 &= J_4 = \omega^2 (1 - \omega) \\ J_2 &= J_3 = J_5 = J_6 = \omega^2 (1 - \xi_1 \omega) \end{aligned}$$

*Elements with a common vertex*

Number of subdomains  $s = 4$ .

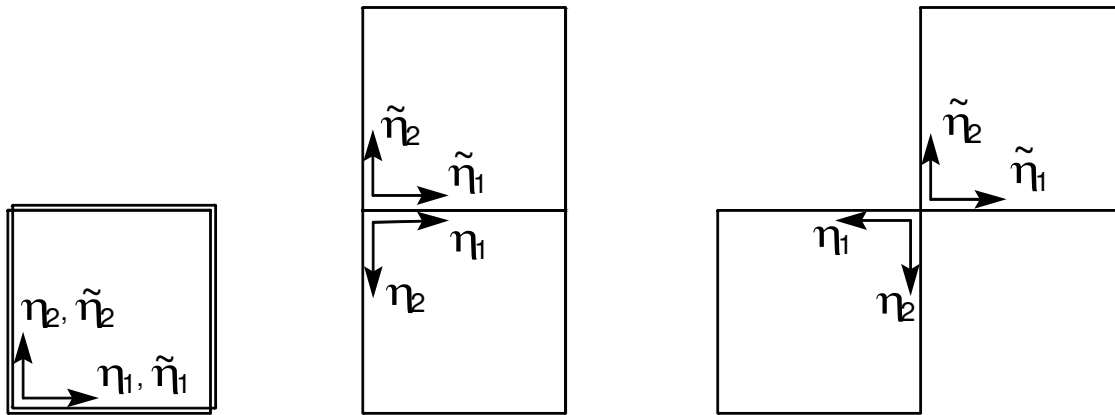


**Figure 3** : Singular cases of integration for a pair of boundary elements: (a) coincident elements, (b) elements with a common edge and (c) elements with a common vertex.

$i$	$\tilde{\eta}_1^i$	$\tilde{\eta}_2^i$	$\eta_1^i$	$\eta_2^i$
1	$v_1$	$v_2$	$v_3$	$v_4$
2	$v_2$	$v_1$	$v_3$	$v_4$
3	$v_2$	$v_3$	$v_1$	$v_4$
4	$v_2$	$v_3$	$v_4$	$v_1$

$$\begin{aligned}
 v_1 &= \omega \\
 v_2 &= \xi_1 \omega \\
 v_3 &= \xi_2 \omega \\
 v_4 &= \xi_3 \omega
 \end{aligned}$$

$$J_i = \omega^3$$

The numerical integration inside each subdomain is performed using the usual Gaussian quadrature integration rule (22), since all the integrals after the appropriate transformations are nonsingular.

### 3 Alternating Method

Using jointly the symmetric Galerkin boundary element method for modeling an arbitrary non-planar crack in an infinite body, and the finite element method for an uncracked finite body, in fracture mechanics problems, allows us to employ advantages of both methods. The finite element method is a robust method for elastic and elastic-plastic problems. It can easily incorporate various types of boundary conditions. The finite element method is widely used in industry. There are commercial preprocessor programs, which are capable of transforming any CAD model into a finite element model.

The boundary element method is most suitable for modeling cracks in infinite bodies. The displacement dis-

continuity approach provides for a simple modeling of the crack. Only one surface of the crack should be discretized. The independence of the crack model and the finite element model of the body allows to easily change the crack model in order to simulate crack growth under monotonic or cyclic loading.

The solution for a finite body with a crack is obtained as a superposition of two models:

1. finite element model for a finite body under external loading, without a crack;
2. an infinite body with a crack modeled by the symmetric Galerkin boundary element method.

Illustration of the superposition principle is presented in Fig. 4. For a correct superposition corresponding to the solution for a finite body with a crack, fictitious forces on the boundary of the finite element model should be found in order to compensate for the stresses caused by the presence of a crack in an infinite body. While this can be done with a direct procedure, the alternating method [Atluri (1997)] provides for a more efficient solution, without assembling the joint SGBEM-FEM matrix.

The SGBEM-FEM alternating method alternates between the finite element solution for an uncracked body and the displacement discontinuity method solution for a crack in an infinite body. Using an iteration procedure, artificial tractions at the boundary of the finite element-modeled body and at the crack surface, are found.

The basic steps of the SGBEM-FEM alternating iteration procedure are as follows:

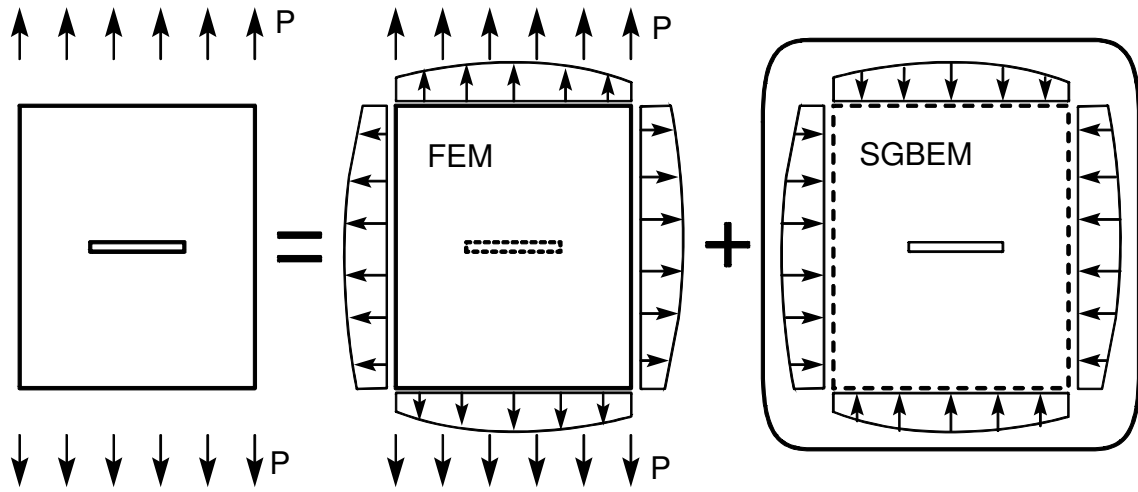


**Figure 4** : Superposition principle: solution for a finite body with a crack can be obtained as a sum of the solution for a finite uncracked body and of the solution for a crack in an infinite body.

1. Using FEM, obtain the stresses at the location of the crack in a finite uncracked body subjected to given boundary conditions.
2. Using SGBEM, solve the problem of a crack, the faces of which subjected to tractions, as found from FEM analysis of the uncracked body.
3. Determine the residual forces at the outer boundaries of the finite body, from displacement discontinuities at the crack surface.
4. Using FEM, solve a problem for a finite uncracked body under residual forces from SGBEM analysis.
5. Obtain the stresses at the location of the crack corresponding to FEM solution.
6. Repeat Steps (2)-(5) until the residual load is small enough.
7. By summing all the appropriate contributions, compute the total solution for a finite body with the crack.

In a matrix notation, the FEM and SGBEM global equation systems look similar:

$$[K_{FEM}]\{u_{FEM}\} = \{P\} \quad (24)$$

$$[K_{BEM}]\{u_{BEM}\} = \{T\} \quad (25)$$

where  $[K_{FEM}]$ ,  $[K_{BEM}]$  are the finite element global stiffness matrix and the boundary element global equation matrix;  $\{u_{FEM}\}$ ,  $\{u_{BEM}\}$  are nodal displacement vectors of the finite element model of the uncracked body and of the boundary element model of the crack surface;  $\{P\}$  is the external load of the finite element model, and  $\{T\}$  are tractions of the boundary element crack model. After the solution of the global equation system, the stresses in the finite element method are computed inside finite elements using the elasticity matrix  $[D]$  and the displacement differentiation matrix  $[B]$ :

$$\{\sigma_{FEM}\} = [D][B]\{u_{FEM}\} \quad (26)$$

The stresses due to displacement discontinuities at the crack surface in the boundary element method are calculated by integration over the crack surface using Eq. (5). This relation in general can be written as:

$$\{\sigma_{BEM}\} = \{\sigma(\{u_{BEM}\})\} \quad (27)$$

The finite element surface residuals  $\{\Psi\}$ , and crack face boundary element tractions  $[T]$ , are estimated through a similar integration:

$$\{\Psi\} = \int_S [N_{FEM}][n]\{\sigma_{BEM}\}dS \quad (28)$$

$$\{T\} = \int_S [N_{BEM}][n]\{\sigma_{FEM}\}dS \quad (29)$$

where  $[N_{FEM}]$ ,  $[N_{BEM}]$  are the finite element and boundary element shape functions, and  $[n]$  are normal vectors to the finite element surface or to the crack surface. Boundary element stresses are used to calculate the finite element residual vector, and vice versa, finite element stresses are involved in the calculation of crack surface tractions. The above SGBEM-FEM alternating procedure can be presented as follows:

$$\begin{aligned} \{u_{FEM}^{(0)}\} &= \{0\} \\ \{\Psi^{(0)}\} &= \{P\} \\ \{u_{BEM}^{(0)}\} &= \{0\} \\ \text{do iterations} \\ \{\Delta u_{FEM}^{(i)}\} &= [K_{FEM}]^{-1} \{\Psi^{(i-1)}\} \\ \{u_{FEM}^{(i)}\} &= \{u_{FEM}^{(i-1)}\} + \{\Delta u_{FEM}^{(i)}\} \\ \{\Delta \sigma_{FEM}^{(i)}\} &= [D][B]\{\Delta u_{FEM}^{(i)}\} \\ \{\Delta T^{(i)}\} &= \int_S [N_{BEM}][n]\{\Delta \sigma_{FEM}^{(i)}\}dS \\ \{\Delta u_{BEM}^{(i)}\} &= [K_{BEM}]^{-1} \{\Delta T^{(i)}\} \\ \{u_{BEM}^{(i)}\} &= \{u_{BEM}^{(i-1)}\} + \{\Delta u_{BEM}^{(i)}\} \\ \{\Delta \sigma_{BEM}^{(i)}\} &= \{\Delta \sigma(\{\Delta u_{BEM}^{(i)}\})\} \\ \{\Psi^{(i)}\} &= \int_S [N_{FEM}][n]\{\Delta \sigma_{BEM}^{(i)}\}dS \\ \text{while } \|\Psi^{(i)}\|/\|P\| &> \varepsilon \end{aligned} \quad (30)$$

#### 4 Calculation of fracture mechanics parameters

In the linear elastic case, the fracture mechanics parameters (stress intensity factors  $K_I$ ,  $K_{II}$  and  $K_{III}$ ) can be easily determined by using asymptotic formulae for displacements in the vicinity of the crack front:

$$\begin{aligned} K_I &= \frac{E}{(1-\nu^2)} \frac{u_3}{4\sqrt{2r/\pi}} \\ K_{II} &= \frac{E}{(1-\nu^2)} \frac{u_2}{4\sqrt{2r/\pi}} \\ K_{III} &= \frac{E}{(1+\nu)} \frac{u_1}{4\sqrt{2r/\pi}} \end{aligned} \quad (31)$$

where  $K_I$ ,  $K_{II}$  and  $K_{III}$  are the stress intensity factors;  $E$  is the elasticity modulus;  $\nu$  is the Poisson's ratio;  $r$  is the

distance from the point to the crack front and  $u_1$ ,  $u_2$  and  $u_3$  are components of the displacement discontinuities at points at the crack surface in a local crack front coordinate system shown in Fig. 5. The axis  $x_1$  of the crack front coordinate system is parallel to the crack front, and the axis  $x_3$  is normal to the crack surface.

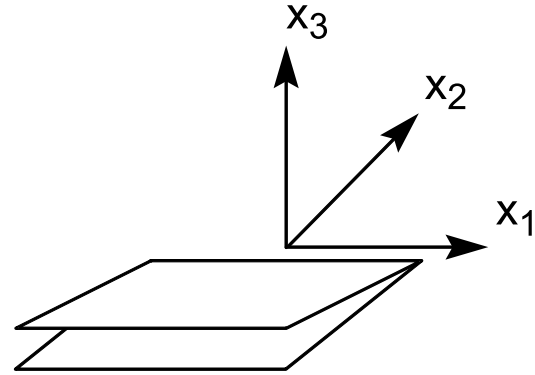


Figure 5 : Local crack front coordinate system

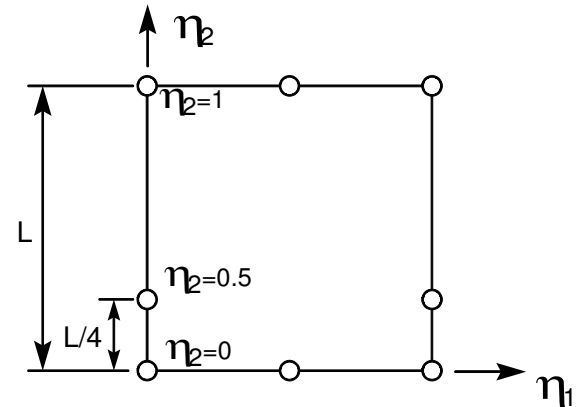


Figure 6 : Singular quarter-point boundary element.

Boundary elements with proper modeling of square-root stress singularity should be used at the crack front, in order to obtain values of the stress intensity factors with good precision. A convenient form of the boundary element with stress singularity is an 8-noded element, with two midside nodes shifted towards the crack front by one quarter of the side length as shown in Fig. 6. The values of  $K_I$ ,  $K_{II}$  and  $K_{III}$  can be determined directly at the quarter point nodes of boundary elements. It is also possible to determine the stress intensity factors by using the

displacement discontinuities at the quarter-point node located at  $L/4$  of the side and at the corner node, which has distance  $L$  along the element side from the crack front.

The following procedure for the stress intensity factor calculation is used in current work:

Obtain the displacement discontinuities  $u_i^G$  in the global coordinate system for the quarter-point node and for the corner node of a singular crack front element;

Extrapolate  $u_i^G/\sqrt{r}$  to the crack front, using values at the quarter-point node ( $L/4$ ) and at the corner node ( $L$ ). Here  $r$  is the distance along line normal to the crack front and  $u_i^G$  are components of displacement discontinuities in the global coordinate system.

Transform the extrapolated displacement discontinuities from the global coordinate system to the crack front coordinate system,  $u_i = \alpha_{ij}u_i^G$  where  $\alpha_{ij}$  are direction cosines of the transformation.

Calculate the stress intensity factors using the equation (31).

### 5 Modeling of Fatigue Crack Growth

SGBEM-FEM alternating method is very suitable for modeling of fatigue crack growth. Since the boundary element model and the finite element model are independent, only the boundary element model (= crack model) should be modified during crack growth modeling.

The crack-front advancement is performed by adding another element layer to the existing crack model. To advance a point at the front of a nonplanar crack it is necessary to know the direction of crack growth and the amount of crack growth. The  $J$ -integral [Cherepanov (1979)] is chosen here as a criterion for fatigue crack growth. According to the  $J$ -integral crack growth criterion:

- (a) Crack grows in the direction of vector  $\Delta\vec{J}$  as shown in Fig. 7;
- (b) Crack growth rate is determined by magnitude of  $\Delta J$ .

In an elastic-plain-strain case, the ranges of  $J$ -integral components are expressed through ranges of the stress intensity factors  $K_I$ ,  $K_{II}$  and  $K_{III}$ :

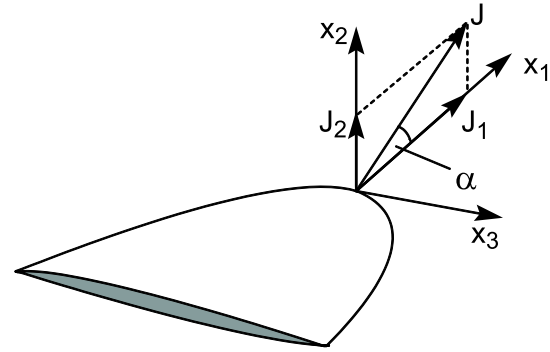


**Figure 7 :**  $J$ -integral components for the crack front point. Crack growth direction is a direction of  $J$ -vector.

$$\begin{aligned} \Delta J_1 &= \frac{1-\nu^2}{E}(\Delta K_I^2 + \Delta K_{II}^2) + \frac{1+\nu}{E}\Delta K_{III}^2 \\ \Delta J_2 &= -2\frac{1-\nu^2}{E}\Delta K_I\Delta K_{II} \\ \Delta J &= \sqrt{\Delta J_1^2 + \Delta J_2^2} \end{aligned} \quad (32)$$

The crack growth angle  $\alpha$  is determined by the direction of  $\Delta\vec{J}$  vector:

$$\tan\alpha = \frac{\Delta J_2}{\Delta J_1} \quad (33)$$

It is worth noting that the  $\Delta\vec{J}$  vector is normal to the crack front. Hence a point at the crack front moves in the plane normal to the crack front at the angle  $\alpha$  from the plane which is tangential to the crack surface.

Typically, material fatigue crack growth models (such as Paris, Forman or NASGRO models) express the functional relationship for crack growth rate through the range of the effective stress intensity factor  $\Delta K_{eff}$ :

$$\frac{da}{dN} = f(\Delta K_{eff}) \quad (34)$$

where  $da/dN$  is the crack growth per cycle and  $\Delta K = K_{max} - K_{min}$ . The range of the effective stress intensity factor  $\Delta K_{eff}$  is related to the range  $\Delta$  by the energy equivalence principle:

$$\Delta K_{eff}^2 = \frac{\Delta J E}{1-\nu^2} \quad (35)$$

Modeling of fatigue crack growth is performed by finite increments. At each increment the maximum crack advance is specified as  $\Delta a_{\max}$ . The crack advance for a particular point at the crack front is calculated as follows:

$$\Delta a = \Delta a_{\max} \frac{(da/dN)}{(da/dN)_{\max}} \quad (36)$$

We use the following procedure for the advancement of the front of a nonplanar crack:

1. Using SGBEM-FEM alternating method, solve the problem for the current crack configuration and determine ranges for the stress intensity factors  $K_I$ ,  $K_{II}$  and  $K_{III}$  for the element corner nodes located at the crack front.
2. For each corner node determine the crack front coordinate system by averaging the coordinate axis vectors determined at the corner point of two neighboring boundary elements.
3. For each corner node, calculate the crack advance  $\Delta a$  using Equation (36) and the crack growth angle according to Equation (33). Move each corner node in the local crack front coordinate system and then transform the movement to the global coordinate system.
4. Find the locations of crack front midside nodes, using cubic spline interpolations for corner nodes from several neighboring elements.
5. Shift the quarter-point nodes of the previous crack front elements to midside position. Put quarter-point nodes on element sides normal to the crack front.

After terminating the crack growth procedure, the total number of cycles  $N$  is calculated as a sum of  $\Delta N_i$  at crack growth increments.

## 6 Numerical Results

The above-presented algorithm of the SGBEM-FEM alternating method has been implemented as a Java code DDFEAM. The Java language has been selected, because of its numerous attractive features: object-oriented nature, simplicity, reliability and portability. The slower

speed of Java, in comparison to C and Fortran, is usually considered to be main obstacle in a wider use of Java for the development of computationally intensive codes. However, at present, Java Virtual Machines, which are used for the execution of Java code, include Just-In-Time compiler and provide reasonable speed for typical multiply-add operations used in computationally intensive routines. A comparison of finite element codes written in C and Java [Nikishkov (2000)] shows that in many cases Java can provide roughly the same performance as the C language. In the worst case, Java is about two times slower than C (this ratio is typical for iterative solvers of equation systems). Our experience indicates that a manual code tuning is more important for Java than for other computer languages. Currently the Java compiler practically does not have actual means for code optimization. Because of this, it is necessary to identify code segments, which consume major computing time and to optimize them manually. In our experience, a manual tuning of the integration routine, for a pair of boundary elements with multiple enclosed loops, produced a ten-times speedup on a Windows computer system. While manual tuning requires some additional efforts, we found that the use of Java leads to an overall development time reduction, because of easier programming and debugging in comparison to other languages.

The developed Java SGBEM-FEM alternating code DDFEAM is applied to the solution of crack problems in infinite and finite bodies. Below we demonstrate the accuracy of the numerical procedure, first for planar and non-planar cracks in infinite media where only SGBEM part of the code is used. Then we present solutions for internal and surface cracks in finite bodies. Finally, an example of fatigue crack growth from an inclined elliptical precrack is given.

In all examples, 8-noded quadrilateral boundary elements are used for crack surface discretization. Gaussian integration rule, with three points in each of the four directions is employed for computing boundary element matrices for regular and singular cases. Quarter-point singular elements are placed at the crack front. Finite element models consist of 20-noded brick-type finite elements.

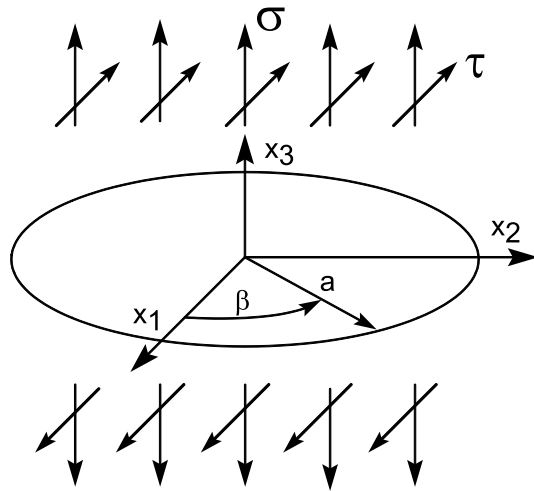


Figure 8 : Penny-shaped crack under uniform tension.

6.1 Penny-shaped crack under tensile and shear loading

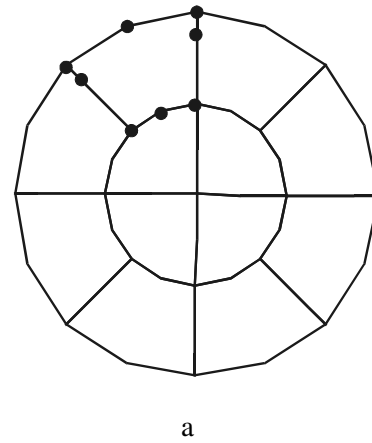
The schematic of the problem for a penny-shaped circular crack under tensile loading along  $x_3$  and shear loading along  $x_1$  is shown in Fig. 8. Exact solution for the problem is given by Sneddon (1946) and Kassir and Sih (1966):

$$K_I = 2\sigma\sqrt{\frac{a}{\pi}}$$

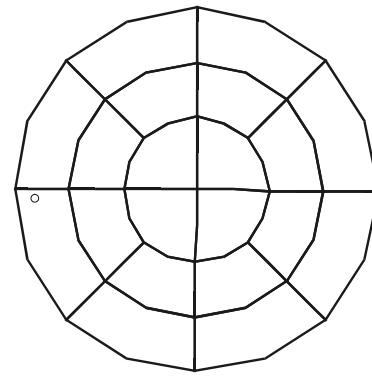
$$K_{II} = \frac{4\tau\cos\beta}{(2-\nu)}\sqrt{\frac{a}{\pi}}$$

$$K_{III} = -\frac{4\tau(1-\nu)\sin\beta}{(2-\nu)}\sqrt{\frac{a}{\pi}}$$

where  $a$  is the crack radius,  $\sigma$  is the applied remote stress,  $\tau$  is the applied shear stress;  $\nu$  is the Poisson's ratio;  $\beta$  is an angle from the direction of shear force on the crack plane. Two meshes consisting of 12 and 20 quadratic elements are used (see Fig. 9). Results for the stress intensity factors normalized as  $K_I/(2\sigma\sqrt{a/\pi})$ ,  $K_{II}/(2\tau\sqrt{a/\pi})$  and  $K_{III}/(2\tau\sqrt{a/\pi})$  are presented in Fig. 10 for the value of Poisson's ratio  $\nu = 0.3$ . Both meshes provide accurate results. The mesh of 20 elements gives values of the stress intensity factors with an error about 0.3% .



a



b

Figure 9 : Meshes for a penny-shaped crack: (a) 12 quadratic elements, (b) 20 quadratic elements.

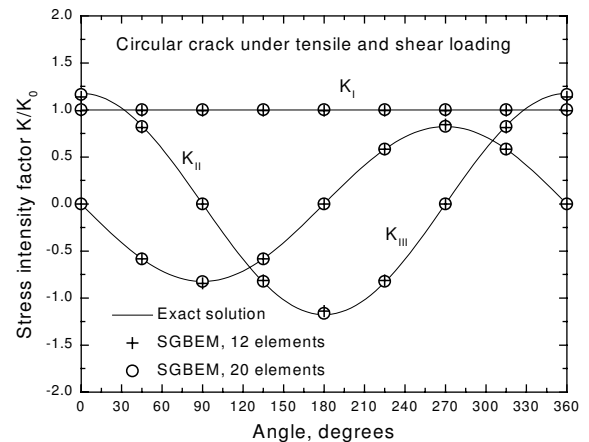


Figure 10 : Stress intensity factors  $K_I, K_{II}$ , and  $K_{III}$  for a penny-shaped crack.

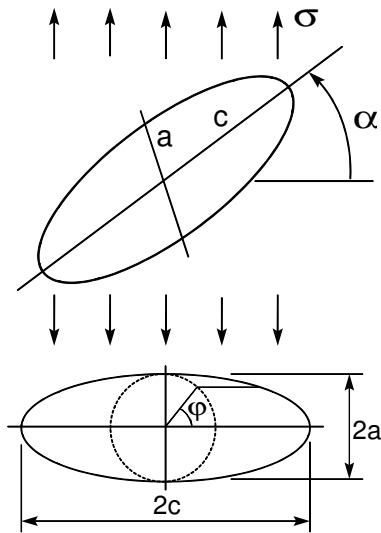


Figure 11 : Inclined elliptical crack under tension.

### 6.2 Inclined elliptical crack under tension

Inclined elliptical crack with semi-axes  $c$  and  $a$  is shown in Fig. 11. The exact solution for a tensile loading  $\sigma$  is given by the relation [Kassir and Sih (1966); Tada, Paris and Irwin (2000)]:

$$K_I = \frac{1}{2}\sigma(1 + \cos 2\alpha) \frac{\sqrt{\pi a} f(\varphi)}{E(k)}$$

$$K_{II} = \frac{1}{2}\sigma \sin 2\alpha \frac{\sqrt{\pi a} k^2 (a/c) \cos \varphi}{B f(\varphi)}$$

$$K_{III} = \frac{1}{2}\sigma \sin 2\alpha \frac{\sqrt{\pi a} k^2 (1 - \nu) \sin \varphi}{B f(\varphi)}$$

$$f(\varphi) = (\sin^2 \varphi + (a/c)^2 \cos^2 \varphi)^{1/4}$$

$$k^2 = 1 - (a/c)^2$$

$$B = (k^2 - \nu)E(k) + \nu(a/c)^2 K(k)$$

where  $\alpha$  is an angle characterizing crack orientation;  $\varphi$  is the elliptical angle and  $K(k)$  and  $E(k)$  are elliptic integrals of the first and second kind:

$$K(k) = \int_0^{\pi/2} \frac{d\varphi}{\sqrt{1 - k^2 \sin^2 \varphi}}, \quad E(k) = \int_0^{\pi/2} \sqrt{1 - k^2 \sin^2 \varphi} d\varphi$$

First, we consider the Mode I case, with the crack-plane being normal to the direction of loading. The two meshes

employed for crack analysis are shown in Fig. 12. Mesh A is composed of 44 boundary elements in such a way that the element edges are normal to the crack front. Mesh B contains 40 boundary elements. It is produced by scaling the circular mesh in one direction. After scaling, the element edges are not normal to the crack front line. Results for the elliptical crack  $a/c = 0.5$  are given in Fig. 13. The stress intensity factor values are normalized as  $K_I/K_I(\pi/2)$ . It can be seen that mesh A with element edges normal to the crack front produces better results than mesh B.

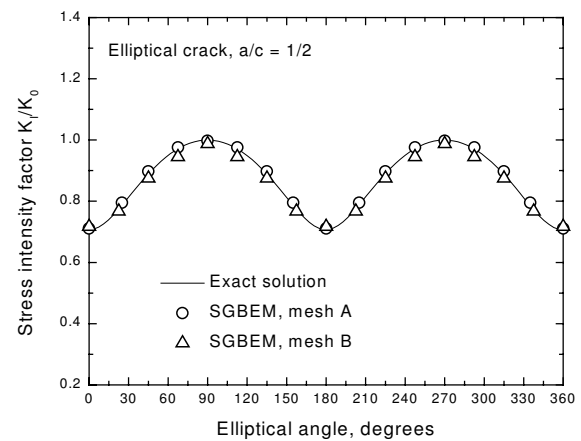
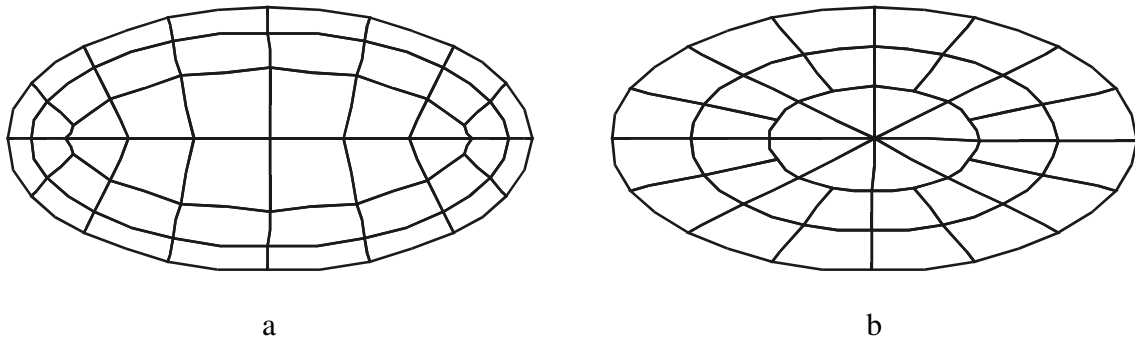


Figure 13 : Stress intensity factor  $K_I$  for an elliptical crack.

The same elliptical crack inclined at 45 degrees, is characterized by the distribution of all three stress intensity factors  $K_I$ ,  $K_{II}$  and  $K_{III}$  along the crack front. Attempts to use same meshes, which were used for mode I analysis, lead to considerable errors in  $K_{II}$  and  $K_{III}$  values for some ranges of elliptical angles. We were not able to obtain good results for  $K_{II}$  and  $K_{III}$  using even refined meshes of type B (Fig. 12). Refined mesh with element sides normal to the crack front is depicted in Fig.14. It is created using elliptical angle increment of 15 degrees. The mesh contains 68 quadratic boundary elements and 229 nodes. SGBEM results for the stress intensity factors  $K_I$ ,  $K_{II}$  and  $K_{III}$  normalized as  $K_i/(\sigma\sqrt{\pi a})$  are presented in Fig. 15. Quite a satisfactory agreement of our results with theoretical solution is observed.

### 6.3 Circular-arc crack under tension

Computation of the stress intensity factors for a circular-arc crack under tensile loading is used as first test for ability of the SGBEM method to model non-planar cracks.



**Figure 12 :** Meshes for an elliptical crack: a) with element edges normal to the crack front, b) with element edges focused to the center of the ellipse.

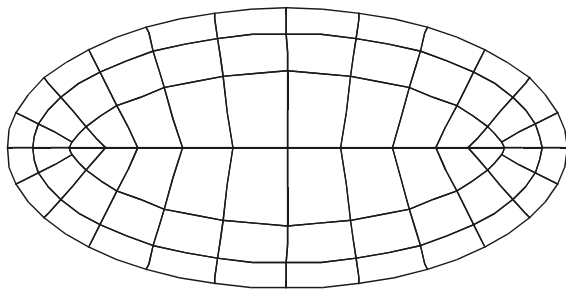


**Figure 14 :** Mesh for an inclined elliptical crack

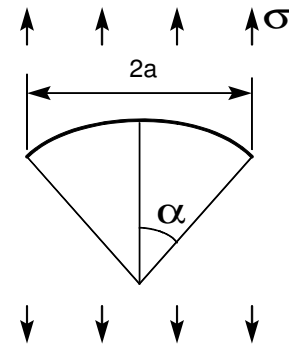


**Figure 16 :** Circular-arc crack under tensile loading

Schematic of the circular-arc crack with a distance between crack tips  $2a$  and an angle  $\alpha$  for half of the arc is presented in Fig. 16. The exact solution for the stress intensity factors  $K_I$  and  $K_{II}$  is given in Reference [Cottrel and Rice (1980)]:

$$K_I = \frac{1}{2} \sigma \sqrt{\pi a} \left( \left( 1 - \frac{1}{4} \sin^2 \alpha \right) \frac{\cos \alpha / 2}{1 + \sin^2 \alpha / 2} + \cos 3\alpha / 2 \right)$$

$$K_{II} = \frac{1}{2} \sigma \sqrt{\pi a} \left( \left( 1 - \frac{1}{4} \sin^2 \alpha \right) \frac{\sin \alpha / 2}{1 + \sin^2 \alpha / 2} + \sin 3\alpha / 2 \right)$$

where  $\sigma$  is the remote tensile stress. This two-dimensional problem is solved as a three-dimensional one using meshes consisting of 60 quadratic elements (typical mesh is shown in Fig. 17). A length of the crack model is chosen as  $10a$ . Stress intensity factors  $K_I$  and  $K_{II}$  calculated at centers of straight crack fronts are compared to the exact solution in Fig. 18. Values of the stress intensity factors are normalized by the factor  $K_0 = \sigma \sqrt{\pi a}$ . Some deviation of computed stress intensity factor  $K_{II}$  from the exact solution is observed only

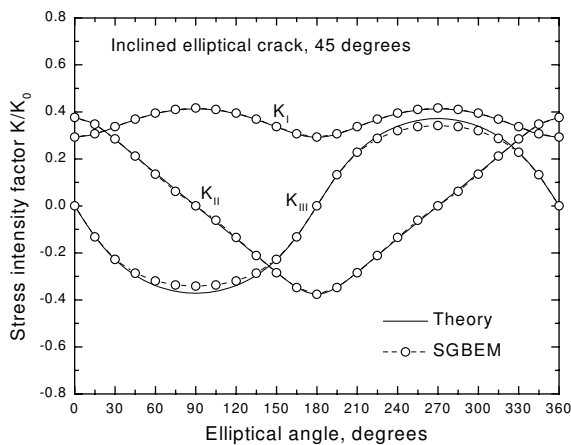


**Figure 15 :** Stress intensity factors  $K_I, K_{II}$  and  $K_{III}$  for an inclined elliptical crack under tension.

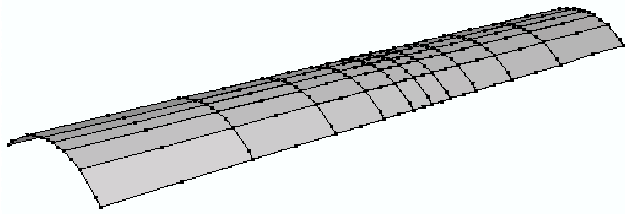


**Figure 17** : Mesh 10 by 16 elements for a circular arc problem.

for large angles  $\alpha$ .

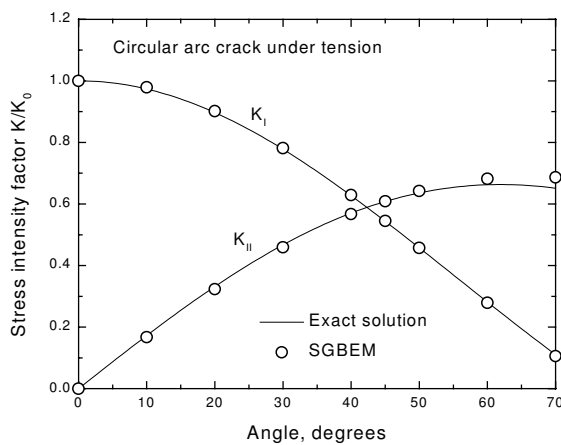


**Figure 18** : Stress intensity factors  $K_I$  and  $K_{II}$  for a circular arc crack.

**6.4 Spherical penny-shaped crack under internal pressure and tension**

A spherical crack bounded by a circular front is shown in Fig. 19. Crack parameters are: a radius of the circular crack front  $a$  and an angle  $\alpha$ . Two load cases are considered: internal crack pressure (Fig. 19,a) and remote tension (Fig. 19,b). A typical mesh of 20 quadratic elements used for calculation of the stress intensity factors  $K_I$  and  $K_{II}$  is presented in Fig. 20. Since the exact solution for the spherical penny-shaped crack is unknown, results are compared to numerical values obtained by Xu and Ortiz (1993) for the Poisson’s ratio  $\nu=0.3$ . Our results for the spherical penny-shaped crack under internal pressure are presented in Fig. 21 as normalized values  $K_I/K_0$  and  $K_{II}/K_0$  where  $K_0 = 2P\sqrt{a/\pi}$  ( $P$  is internal pressure). Good agreement between our results and results of Reference [Xu and Ortiz (1993)] is observed for the case of internal pressure.

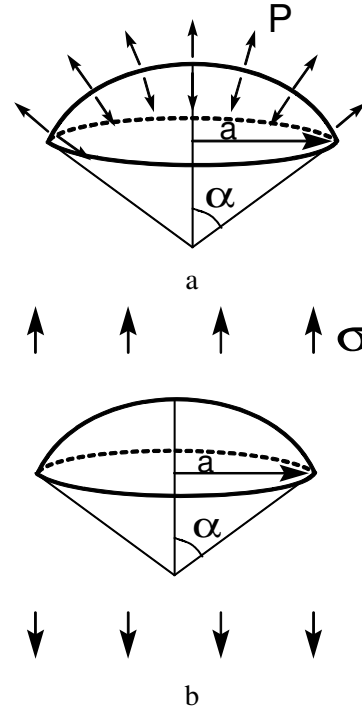


**Figure 19** : Spherical penny-shaped crack under internal pressure (a) and tensile loading (b).

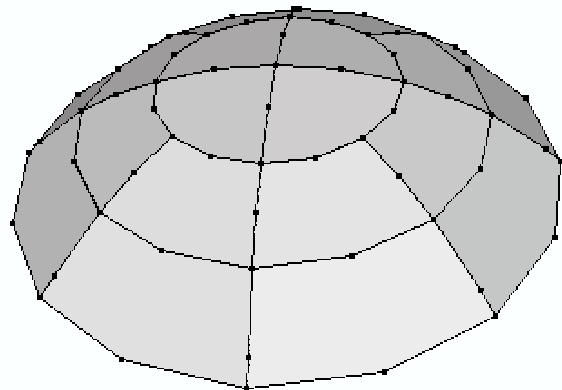


**Figure 20** : Mesh for a spherical penny-shaped crack.

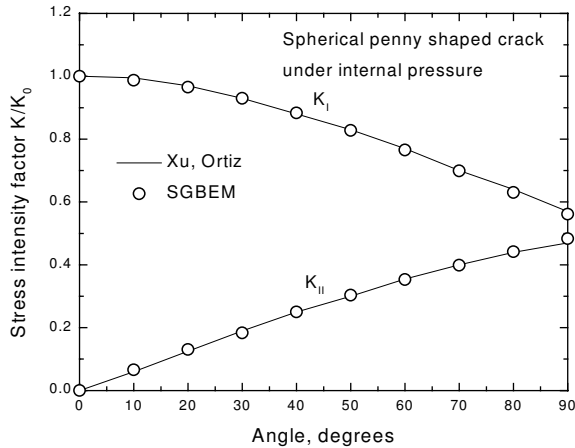


Figure 21 : Stress intensity factors  $K_I$  and  $K_{II}$  for a spherical penny shaped crack under internal pressure.

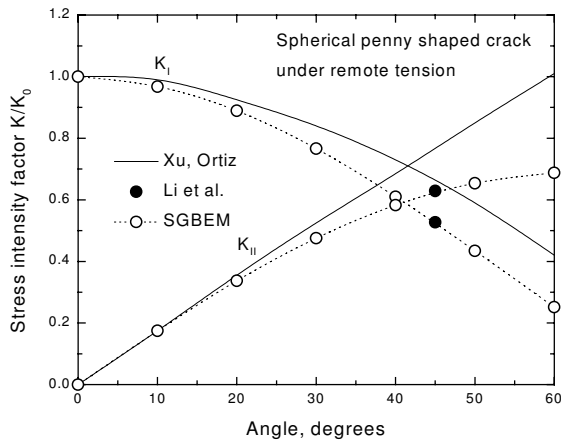


Figure 22 : Stress intensity factors  $K_I$  and  $K_{II}$  for a spherical penny shaped crack under remote tension.

The stress intensity factors  $K_I$  and  $K_{II}$  normalized by  $K_0 = 2\sigma\sqrt{a/\pi}$  for the spherical crack under remote tension obtained with the use of our code and those from References [Xu and Ortiz (1993)] and [Li, Mear and Xiao (1998)] are shown in Fig 22. Our results for the stress intensity factor  $K_I$  and  $K_{II}$  are in agreement with the results of Li, Mear and Xiao (1998) for  $\alpha= 45$  degrees. Deviation of our values of the stress intensity factors from the results of Xu and Ortiz (1993) is considerable. Taking into account that our results are supported by results of Reference [Li, Mear and Xiao (1998)] and that Xu and Ortiz give unrealistically high values of  $K_{II}$  for large angles  $\alpha$ , we conclude that results of Xu and Ortiz may contain some errors.

6.5 Embedded circular crack in a cylindrical bar and in a cube

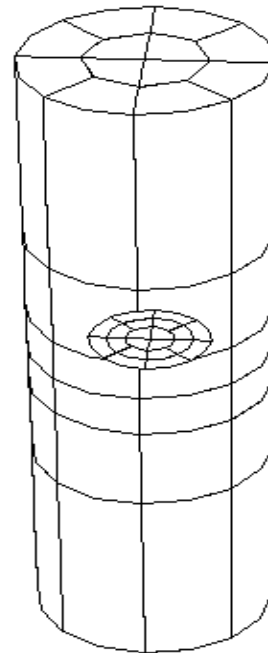
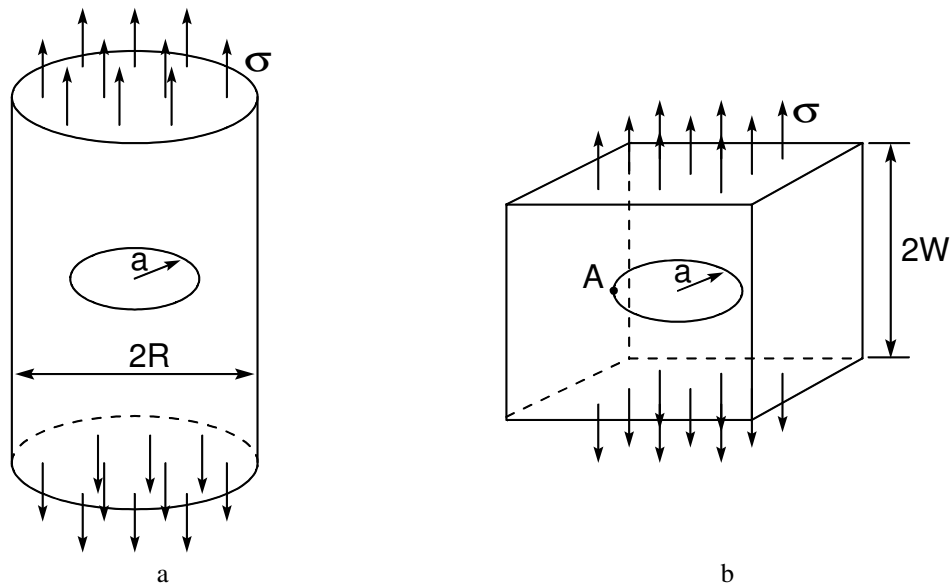


Figure 24 : Finite element-boundary element model for a cylinder bar with an inner circular crack.

Two problems for embedded cracks in finite bodies, include a circular crack inside a cylindrical bar (Fig. 23,a) and a circular crack embedded in a cube (Fig. 23,b). For a circular bar with an embedded circular crack, a discrete model shown in Fig. 24 is used. This discrete model consists of the finite element model (72 brick-type 20-noded elements) and the boundary element model (20 quadri-



**Figure 23 :** Inner circular crack in a cylindrical bar (a) and in a cube (b).

lateral 8-noded elements). The solution for a finite body with a crack was obtained by the alternating method. The number of iterations inside the alternating procedure varies from 3 for a crack  $a/R = 0.3$  to 6 for a crack  $a/R = 0.8$ . A comparison of the stress intensity factors normalized by  $K_0 = 2\sigma\sqrt{a/\pi}$  obtained by of SGBEM-FEM alternating method with the approximated solution of Reference [Tada, Paris and Irwin (2000)] is presented in Fig. 25.

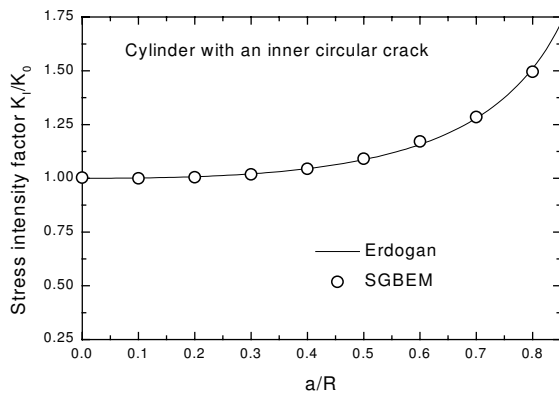


**Figure 25 :** Stress intensity factor  $K_I$  for a circular crack in a cylindrical bar under tension.

Finite element – boundary element model used for analyzing circular crack in a cube under tensile loading is shown in Fig. 26. The finite element model consists of

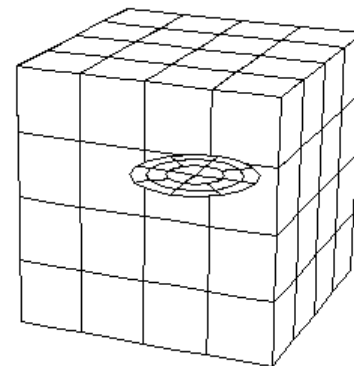


**Figure 26 :** Finite element-boundary model for a cube with an inner circular crack.

64 elements. Three boundary element meshes consisting of 12, 20 and 40 elements are used (mesh of 20 elements is depicted in Fig. 26). Dependence of the results for the stress intensity factor  $K_I$  on the number of elements in the boundary element model is presented in Table 1 where also given  $K_I$  value obtained by Li, Mear and Xiao (1998).

**6.6 Semi-circular and semi-elliptical surface cracks**

Since the ability to model surface cracks is important from a practical point of view, the present SGBEM-FEM alternating method is next applied to problems involving semi-circular and semi-elliptical surface cracks. Fig. 27

**Table 1** : Stress intensity factor for circular crack in a cube under tension

Number of boundary elements	$K_I/(\sigma\sqrt{\pi a})$
12	2.178
20	2.206
40	2.213
[Li, Mear and Xiao (1998)]	2.213

shows a semi-elliptical surface crack in a plate subjected to a uniform tensile stress  $\sigma$ . The crack is characterized by semi-axis ratio  $a/c$  and by relative depth  $a/t$  and width  $a/W$ .

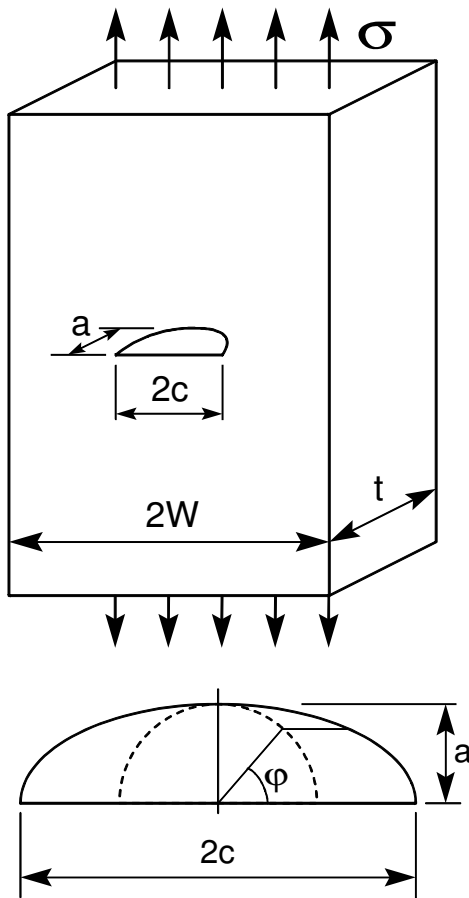


**Figure 27** : Semi-elliptical surface crack in a plate.

First, we analyze a semi-circular surface crack with  $a/c = 1$ ,  $a/t = 1/3$  and  $W = t$ . The finite element-boundary element model is shown in Fig. 28. The finite element model contains 192 quadratic 20-noded elements. The crack model consists of 20 boundary elements. An at-

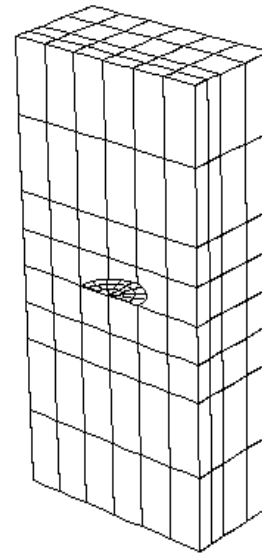


**Figure 28** : Finite element-boundary element model for a semi-circular crack in a plate.

tempt to solve the problem using finite element-boundary element model presented in Fig. 28 with a crack modeled as in Fig. 29,a lead to a slightly higher than expected values of the stress intensity factor  $K_I$ . From physical point of view the reason is quite clear. The finite element model for the uncracked body, and the boundary element model for the crack, are connected through residual forces. Because of this, edges of crack surfaces on the body surface can have excessive rotations, thus leading to higher stress intensity factors at the crack front. We propose a simple approach, which helps to decrease the rotation of crack surfaces at the surface of the body. According to this approach, for a surface crack, it is necessary to add a fictitious portion of the crack surface outside the body, as shown in Fig. 29,b. It was found that a reasonable additional crack surface can have an area, which is equal to the crack area, and can consist of one row of boundary elements. Since, geometrically, the additional crack surface is very simple, it can be generated automatically during the program run. Values of the stress intensity factor for a semi-circular surface crack obtained with the use of the crack mesh of Fig. 29,b are shown in Fig. 30. The stress intensity factor is normalized as  $K_I/K_0$  where  $K_0$  is equal:

$$K_0 = \sigma\sqrt{\frac{\pi a}{Q}}, \quad Q = 1 + 1.464\left(\frac{a}{c}\right)^{1.65}$$

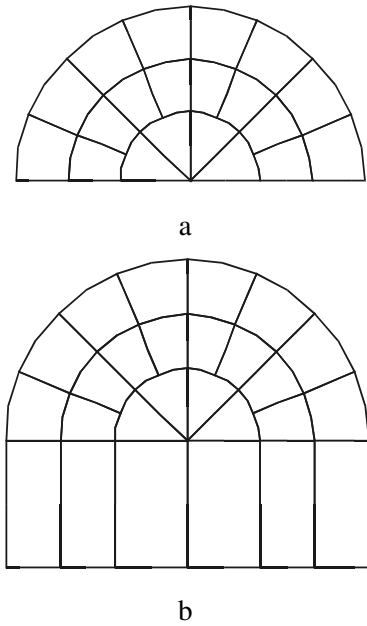


**Figure 29** : Boundary element model for a semi-circular crack: a) generated by the user, b) actually used in SGBEM-FEM alternating procedure

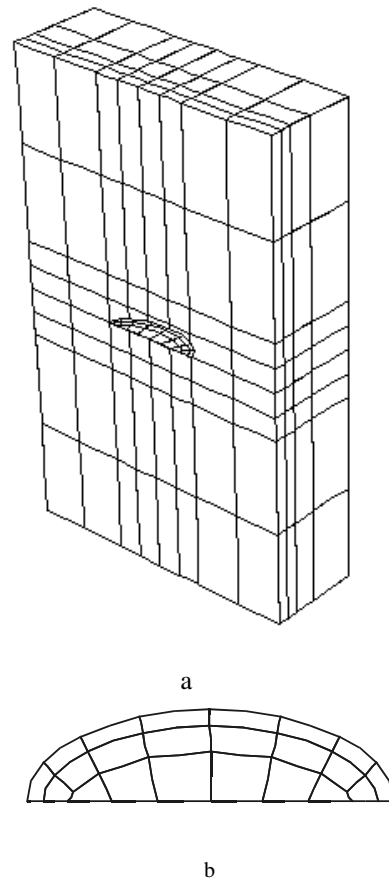


**Figure 31** : Finite element-boundary element model for a semi-elliptical surface crack in a plate (a) and boundary element mesh for a crack (b).

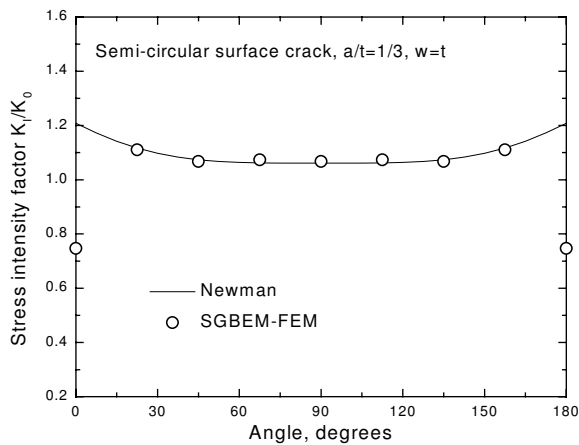


**Figure 30** : Stress intensity factor  $K_I$  for a semi-circular surface crack in a plate under tension.

A comparison of the SGBEM-FEM results with those given by Newman and Raju (1984) shows their good agreement for all angles except at points where the crack front approaches free surface of the body. The effect of the rapid decrease of  $K_I$  in a thin layer near the free boundary is known (see, for example, Reference [Li, Mear and Xiao (1998)]). This effect is usually neglected in publications containing approximate equations for the stress intensity factor  $K_I$ .

Fig. 31 shows a finite element model (256 brick-type elements) and a crack model (22 boundary elements) for analyzing surface semi-elliptical crack  $a/c = 1/2$ ,  $a/t = 1/4$  and  $W = 2t$ . Normalized values of the stress intensity factor  $K_I$  (normalization is same as for the semi-circular crack) are presented in Fig. 32 along with finite element results from Reference [Wu (1984)]. Again a good agreement is observed except points on the free surface.

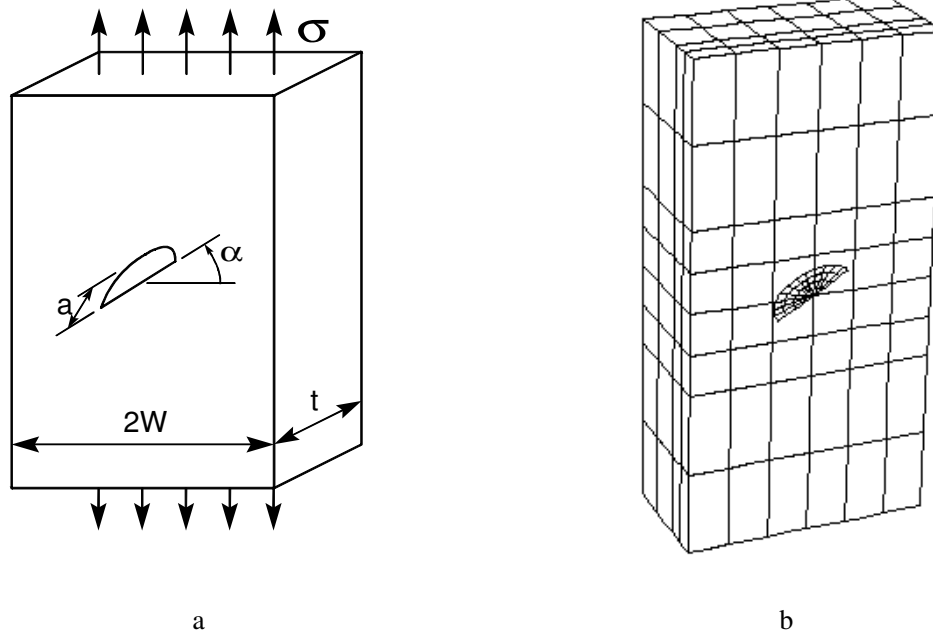


**Figure 33 :** Inclined semi-circular surface crack in a plate (a) and a finite-element boundary-element model of the problem (b).

**6.7 Inclined semi-circular surface crack in a plate**

A plate with an inclined semi-circular surface crack was analyzed. The crack plane is oriented at an angle  $\alpha = 30^\circ$  to a cross-sectional plane of the plate as shown in Fig. 33,a. Other problem parameters are: the relative crack depth  $alt = 1/3$ ,  $W = t$  and the Poisson's ratio  $\nu = 0.3$ . A discrete model used is presented in Fig. 33,b. The finite element model contains 192 20-noded brick-type elements. The boundary element model of a crack consists of 50 quadratic elements (42 elements for crack itself plus 8 elements for fictitious crack surface outside body). Results for the stress intensity factors  $K_I$ ,  $K_{II}$  and  $K_{III}$  normalized as  $K_i / (\sigma\sqrt{\pi a})$  are presented in Fig. 34. Numerical results for same orientation of an inclined semi-circular surface crack have been reported by Shivakumar and Raju (1992) and by He and Hutchinson (2000). Some differences between solution obtained here and previously reported results exist only for points of the crack front, which are located at the free surface of the structure.

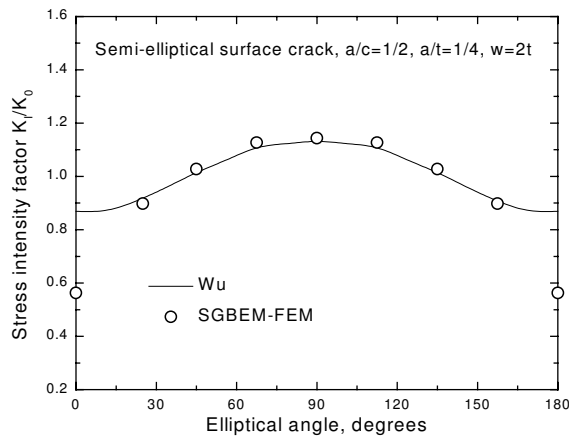


**Figure 32 :** Stress intensity factor  $K_I$  for a semi-elliptical surface crack in a plate under tension.

**6.8 Nonplanar fatigue crack growth**

The fatigue growth of a nonplanar crack under mixed-mode loading conditions is performed starting from an inclined elliptical precrack subject to a uniform tensile

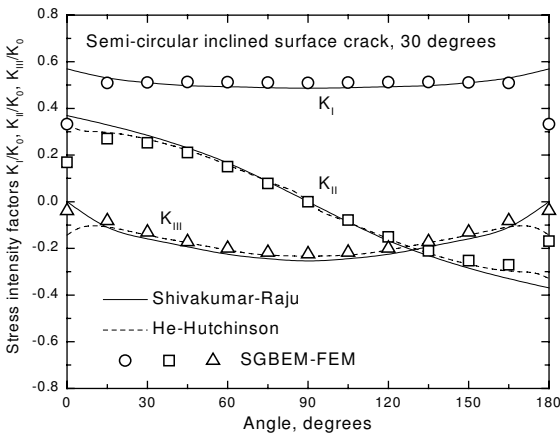


**Figure 34 :** Stress intensity factors  $K_I$ ,  $K_{II}$ , and  $K_{III}$  for an inclined semi-circular surface crack in a tensile plate.

loading (Fig. 11). An ellipse with major semi-axis ratio  $a/c = 0.5$  and orientation  $\alpha = 45^\circ$  is used as a precrack. The precrack is discretized by 68 quadratic boundary elements as shown in Fig. 14. The Paris material fatigue model was chosen to simulate fatigue crack growth:

$$\frac{da}{dN} = c(\Delta K_{eff})^m$$

where  $da/dN$  is the crack growth rate with respect to the loading cycles,  $c = 1.49 \cdot 10^{-8}$  and  $m = 3.321$  are material parameters for 7075 Aluminum.

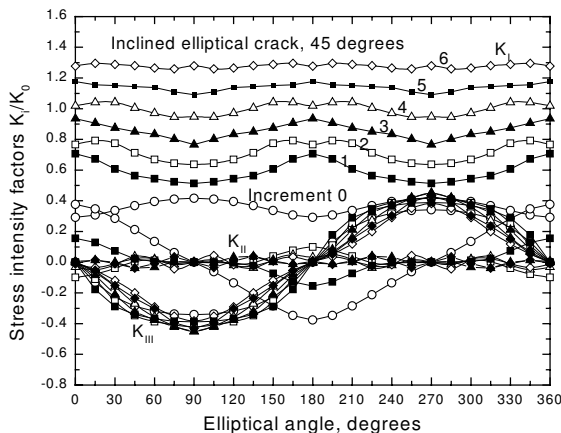


**Figure 35 :** Stress intensity factors  $K_I$ ,  $K_{II}$ , and  $K_{III}$  for an inclined elliptical crack after crack growth increments 1-6.

First, the elliptical precrack is analyzed and the stress intensity factors  $K_I$ ,  $K_{II}$  and  $K_{III}$  are calculated for the

crack front nodes. According to the  $J$ -integral vector orientation and magnitude, points at the crack front are advanced to new positions with scaling to the specified maximum crack advance  $da_{max}$ . A new layer of elements is generated between old and new crack front lines. Then the new crack model is analyzed and *etc.* Six crack advancements with specified  $da_{max}/a = 0.3, 0.4, 0.5, 0.6, 0.7$  and  $0.8$  were performed. Stress intensity factors  $K_I$ ,  $K_{II}$  and  $K_{III}$  after crack increments are given in Fig. 35 with normalization  $K_i/(\sigma\sqrt{\pi a})$ . A three-dimensional view of the crack after six increments and its projections on planes XZ and XY are presented in Fig. 36. While it is not possible compare results precisely, our distributions of the stress intensity factors along crack front during crack growth are similar to those published in Reference [Mi and Aliabadi (1994)]. And the shape of the final crack is alike to crack shapes obtained by other researchers [Mi and Aliabadi (1994); Forth and Keat (1997)].

### 7 Conclusion

An SGBEM-FEM alternating method has been developed for the analysis of non-planar cracks in finite bodies. The symmetric Galerkin boundary element method is used for the solution of a problem for a crack in an infinite medium. A body without a crack is modeled by the finite element method. The solution of a problem for a finite body containing a crack is sought by alternating between SGBEM solution for a crack and FEM solution for an uncracked body. Usually less than 10 iterations are enough for convergence. Since the finite element mesh for the uncracked body and the boundary mesh for the crack are completely independent, the SGBEM-FEM alternating method is particularly efficient for modeling of fatigue crack growth.

Because the crack is represented as a distribution of displacement discontinuities only one crack surface needs to be discretized. The symmetric Galerkin boundary element method involves weakly singular integration for element pairs. Special transformations in a four-dimensional space, help to make integrals regular; thus allowing one to apply usual Gaussian quadrature rule for their evaluation. Quadratic 8-noded elements are used for discretization of the crack surface. These elements provide good accuracy and can be easily transformed into singular elements by moving midside nodes to quarter-side positions.

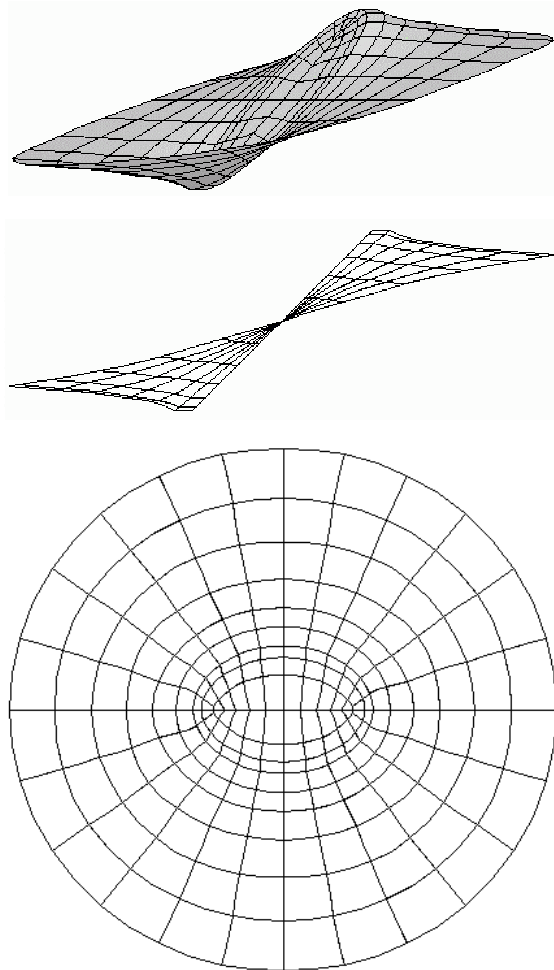


**Figure 36** : Crack after 6 crack front advances: 3D view and projections on planes XZ and XY.

The accuracy and efficiency of the SGBEM-FEM alternating procedure is demonstrated by solving examples for planar and non-planar cracks in infinite media and for inner and surface cracks in finite bodies. An example of fatigue crack growth from an inclined elliptical precrack is given.

**Acknowledgement:** Various parts of the work were supported, over the years, by FAA, ONR, and NASA. The authors thank Drs. Dy Le, Yapa Rajapakse, and Ivatury Raju, for their encouragement and support.

### References

**Andra, H.** (1998): Integration of singular integrals for the Galerkin-type boundary element method in 3D elasticity. *Comp. Methods Appl. Mech. Engng*, vol. 157, pp. 239-249.

**Atluri S.N.** (1997): *Structural Integrity and Durability*, Tech Science Press, Forsyth.

**Atluri, S.N.; Zhu, T.** (1998): A new meshless local Petrov-Galerkin (MLPG) approach in computational mechanics, *Computational Mechanics*, vol.22, pp. 117-127.

**Bonnet, M.; Maier, G.; Polizzotto, C.** (1998) Symmetric Galerkin boundary element methods. *Appl. Mech. Rev.*, vol. 51, pp. 669-704.

**Cherepanov, G.P.** (1979): *Mechanics of Brittle Fracture*, McGraw-Hill, New York.

**Cisilino, A.P.; Aliabadi, M.H.** (1999): Three-dimensional boundary element analysis of fatigue crack growth in linear and non-linear fracture problems. *Eng. Fract. Mech.*, vol. 63, pp. 713-733.

**Cotterel, B.; Rice, J.R.** (1980): Slightly curved or kinked cracks. *Int. J. Fracture*, vol. 16, p.155.

**Erichsen, S.; Sauter, S.A.** (1998): Efficient automatic quadrature in 3-d Galerkin BEM. *Com. Methods Appl. Mech. Engng*, vol. 157, pp. 215-224.

**Forth, S.C.; Keat, W.D.** (1997): Nonplanar crack growth using the surface integral method. *Transactions*

of the ASME. *Journal of Engineering for Gas Turbines and Power*, vol. 119, pp. 964-968.

**Frangi, A.; Novati, G.; Springhetti, R.; Rovizzi, M.** (2000): Fracture mechanics in 3D by the symmetric Galerkin boundary element method. *VIII Conf. On Numerical Methods in Continuum Mechanics, 19-24 Sept. 2000, Liptovsky Jan, Slovak Republic.*

**He, M.Y.; Hutchinson, J.W.** (2000): Surface crack subject to mixed mode loading. *Eng. Fract. Mech.*, vol. 65, pp. 1-14.

**Kassir, M.K.; Sih, G.C.** (1966): Three-dimensional stress distribution around an elliptical crack under arbitrary loading. *Journal of Appl. Mech.*, vol. 33, pp. 601-611.

**Keat, W.D.; Annigeri, B.S.; Cleary, M.P.** (1988): Surface integral and finite element hybrid method for two- and three-dimensional fracture mechanics analysis. *Int. J. Fracture*, vol. 36, pp. 35-53.

**Kim, H.G.; Atluri, S.N.** (2000): Arbitrary placement of secondary nodes and error control in the meshless local Petrov- Galerkin (MLPG) method, *Computer Modeling in Engineering & Sciences*, vol. 1,3, pp. 11-32.

**Li, S.; Mear, M.E.** (1998): Singularity-reduced integral equations for displacement discontinuities in three-dimensional linear elastic media. *Int. J. Fract.*, vol. 93, pp. 87-114.

**Li, S.; Mear, M.E.; Xiao, L.** (1998): Symmetric weak-form integral equation method for three-dimensional fracture analysis. *Comput. Meth. Appl. Mech. Engng*, vol. 151, pp. 435-459.

**Lin, H.; Atluri, S.N.** (2000): Meshless local Petrov-Galerkin (MLPG) method for convection – diffusion problems, *Computer Modeling in Engineering & Sciences*, vol. 1,2, pp. 45-60, 2000.

**Mi, Y.; Aliabadi, M.H.** (1994): Three-dimensional crack growth simulation using BEM. *Computers & Structures*, vol. 52, pp. 871-878.

**Newman, J.C.; Raju, I.S.** (1984): *Stress-Intensity Factor Equations for Cracks in Three-Dimensional Finite Bodies Subjected to Tension and bending Loads.* NASA Technical Memorandum 85793, NASA Langley Research Center, Hampton, VA.

**Nikishkov, G.P.** (2000): Performance of a finite element code written in Java. *Advances in Computational Engineering & Sciences 2000 (Ed. S.N.Atluri and F.W.Brust), V.1.* Tech Science Press, Palmdale, CA, pp. 264-269.

**Nikishkov, G.P.; Atluri, S.N.** (1987): Calculation of fracture mechanics parameters for an arbitrary three-dimensional crack by the ‘equivalent domain integral’ method. *Int. J. Numer Meth. Engng*, vol. 24, pp. 851-867.

**Nishioka, T.; Atluri, S.N.** (1983): Analytical solution for embedded elliptical cracks and finite element – alternating method for elliptical surface cracks, subjected to arbitrary loadings. *Eng. Fract. Mech.*, vol. 17, pp. 247-268.

**Shivakumar, K.N.; Raju, I.S.** (1992): An equivalent domain integral method for three-dimensional mixed-mode fracture problems. *Eng. Fract. Mech.*, vol. 42, pp. 935-959.

**Sneddon, I.N.** (1946): The distribution of stress in the neighborhood of a crack in an elastic solid. *Proceedings of the Royal Society of London, Ser A* 187, pp. 229-260.

**Tada, H.; Paris, P.C.; Irwin, G.R.** (2000): *The Stress Analysis of Cracks Handbook*, ASME Press.

**Vijaykumar, K.; Atluri, S.N.** (1981): An embedded elliptical crack, in an infinite solid, subject to arbitrary crack-face tractions,” *J. Appl. Mech.*, vol. 103(1), pp. 88-96.

**Wu, X.R.** (1984): Stress intensity factors for half-elliptical surface cracks subjected to complex crack face loading. *Eng. Fract. Mech.*, vol. 19, pp. 387-405.

**Xu, G.; Ortiz, M.** (1993): A variational boundary integral method for the analysis of 3-D cracks of arbitrary geometry modelled as continuous distribution of dislocation loops. *Int. J. Numer. Meth. Eng.*, vol. 36, pp. 3675-3701.